Vapor Phase Infiltrated AlOx/PIM-1 "Hybrid Scaffolds" as Solution-Processable Amine Supports for CO_2 Adsorption

Fengyi Zhang,[a] Emily K. McGuinness,[b] Yao Ma,[a] Yi Ren,[a] Johannes E. Leisen,[c] Mark D. Losego,[b] and Ryan P. Lively[a]*

a. School of Chemical and Biomolecular Engineering, Georgia Institute of Technology, Atlanta, GA 30332, USA.

b. School of Materials Science and Engineering, Georgia Institute of Technology, Atlanta, GA 30332, USA

c. School of Chemistry and Biochemistry, Georgia Institute of Technology, Atlanta, GA 30332, USA

KEYWORDS. CO_2 capture, polymer of intrinsic microporosity, vapor phase infiltration, adsorption, adsorption kinetics.

ABSTRACT. Energy-efficient adsorptive CO_2 capture requires both adsorbent materials with high CO_2 capacity and structured adsorption contactors possessing fast mass transfer kinetics and low pressure drop. State-of-the-art research primarily focuses on "hard" adsorbents such as

mesoporous zeolites and metal-organic frameworks, which exhibit high CO_2 capacities but are challenging to translate into structured contactors. PIM-1, a solution-processable microporous polymer, is a "softer" alternative that can be easily fabricated into structured adsorption contactors. In prior research, PIM-1 has been utilized as a "molecular basket" for poly(ethylene imine) (PEI). Despite nanoscale amine dispersion and excellent processability, PEI/PIM-1 composites possess an unstable micropore structure, which collapses at high PEI loadings (~ 30%) and results in lower CO_2 adsorption capacity than PEI-loaded hard oxides. Here, we applied a post-fabrication polymer stabilization method, vapor phase infiltration (VPI), to improve the CO_2 capacity for PEI/PIM-1 composite without sacrificing its processibility. PIM-1 is fabricated into structured adsorption contactors and then reinforced with amorphous aluminium oxyhydroxide (AlO_x) nanostrands via VPI. The resulting AlO_x/PIM-1 is a stable, hierarchically porous support, which can be loaded with 40% PEI without pore collapse. Owing to the combination of processibility, comparable CO_2 capacity, and high amine efficiency, PEI/AlO_x/PIM-1 composites are a promising alternative to PEI-loaded mesoporous oxides.

1. Introduction

Cost-effective CO_2 capture techniques are needed to combat rising atmospheric CO_2 concentrations that contribute to global warming.[1-3] Currently, CO_2 capture from large point sources (e.g., power plants) is achieved via amine-based scrubbing.[4] These liquid-based sorption technologies require advanced heat integration and suffer from amine degradation, volatile emissions, and high energy penalty due to latent heat of solvents.[5, 6]

A promising alternative CO_2 capture technique is adsorption via solid CO_2 sorptive materials. Compared with liquid-based scrubbing, solid adsorbents are inherently more energy efficient owing to low heat capacity and absence of solvent phase change. The performance of the adsorption process is determined by not only the adsorbent material but also the adsorption contactor design, which plays an important role in heat management, pressure drop, and mass transfer rates.[7-9] State-of-the-art adsorbent materials include silica- or alumina-based porous materials grafted or impregnated with amine-containing molecules,[10] amine-loaded mesoporous zeolites,[1, 11] diamine-appended metal-organic frameworks,[12] among others. Due to their inherently low processibility, these inorganic adsorbents are usually produced as powder or pellets and then used as a fluidized bed or a fixed bed, which results in challenging heat management, the trade-off between mass transfer rate and pressure drop, and particle attrition.[7]

In order to fabricate adsorption contactors with optimized structures,[8, 13] it is important to develop adsorbent materials compatible with scalable material processing techniques.[14, 15] Polymer of intrinsic microporosity 1 (PIM-1) contains significant amount of intrinsic micropores (by IUPAC definition, micropores refer to pores with diameters less than 2 nm) that could disperse PEI into nanosized domains and effectively minimize the kinetic limitation of CO_2 capture.[16] As a solution-processable microporous material, PIM-1 can be dissolved in common organic solvents (e.g., tetrahydrofuran) and fabricated into various mass transfer contactors, such as fiber sorbents.[5, 8, 17-19] The structured PIM-1 adsorbent can then be loaded with amine molecules with a better dispersion than classical amine-loaded mesoporous silica or alumina, which translates into outstanding amine efficiency.[5] The combination of processibility and amine efficiency makes PEI/PIM-1 composites promising CO_2 adsorbents.[5] However, the linear polymer structure of PIM-1 is subject to plasticization from PEI. Overloading of PEI into PIM-1 will result in the collapse

of the adsorber architecture and a subsequent reduction of amine efficiency.[5] To effectively disperse and expose amine groups, PIM-1 must be protected against plasticization to provide stable support for PEI. One strategy to stabilize microporous polymers without damaging the polymer microstructure is post-fabrication vapor phase infiltration (VPI).[17, 20] Vapor phase infiltration is hypothesized to create a hybrid material of intertwined PIM-1 polymer chains and alumina-based nanostrands (AlO_x), which prevent the PIM-1 polymer chains from relaxing, swelling, or partaking in other large scale motions in the presence of guest molecules. The resulting AlO_x/PIM-1 composite exhibits significantly improved microstructural stability, even in the presence of strong solvents (e.g., chloroform, tetrahydrofuran, methanol, etc.).[17]

In this work, new composite PEI/AlO_x/PIM-1 adsorption contactors are created as demonstrated in **Scheme 1**. Hierarchically porous PIM-1 contactors are fabricated via solution-based processing technique (e.g., fiber spinning), pretreated by methanol, and then undergo two cycles of VPI treatment at 90˚C with trimethylaluminium (TMA) and water vapor as co-reactant.[8, 18, 19] The resulting AlO_x/PIM-1 contactor is then loaded with amine molecules (e.g., branched PEI) via wet impregnation.[5] In this report, these PEI/AlO_x/PIM-1 composites are explored for CO_2 capture applications with detailed analysis of the inorganic structure as well as adsorption phenomena.

2. Experimental Section

2.1. PIM-1 synthesis

The PIM-1 synthesis procedure has been described in prior publications.[17, 21] Briefly, purified tetrafluoroterephthalonitrile (TFTPN, Alfa Aesar) and 5,5′,6,6′-tetrahydroxy- 3,3,3′,3′-tetramethyl-1,1′-spirobisindane (TTSBI, Alfa Aesar) undergo polymerization in the presence of potassium carbonate fine powder and anhydrous DMF at 65 °C for 72 hours. H_2O is added into the synthesis mother solution to dissolve the remaining potassium carbonate and quench out PIM-

1. The PIM-1 is then dried and dissolved by chloroform and quenched out by methanol. After that, PIM-1 was washed by DMF and methanol sequentially to remove unreacted monomers and oligomers. Mn of the PIM-1 used in this study is 50,200 Da with Mw/Mn around 1.65 as analyzed by GPC.

2.2. Hierarchically porous PIM-1 fibers fabrication

Hierarchically porous PIM-1 fibers were produced via evaporation-induced phase inversion.[8, 18] The polymer solution composition was PIM-1: THF (tetrahydrofuran) :DMAc (dimethylacetamide) = 10:23:17. The polymer solution is extruded through a stainless-steel needle (G24, the inner diameter 311 μm) driven by 300 kPa nitrogen supplied by a gas cylinder. PIM-1 fibers were deposited onto a glass stage. A THF-saturated nitrogen sweep over the freshly-deposited PIM-1 was used to prevent the formation of dense skin layer and structure collapsing.[18] The resulting solvent-saturated PIM-1 fibers were then naturally dried in ambient conditions. Subsequent vacuum drying (80 °C, 85 kPa vacuum, 12 hr) was conducted to remove solvent residue.

2.3. Vapor phase infiltration

Vapor phase infiltration was carried out following the procedure detailed in our previous publication.[17] Briefly, prior to infiltration, PIM-1 samples were soaked in methanol for 2 hours to reset the processing history and then dried in a fume hood for 30 minutes.[21] In an evacuated reactor, the PIM-1 samples were exposed to trimethylaluminum, water, trimethylaluminum, and water sequentially at 90 ºC. Each exposure lasted for 5 hours for thorough infiltration and was separated by a 5 minute nitrogen purge and 5 minute pump down to rough vacuum (Figure S1).

2.4. Thermogravimetric analysis

Thermogravimetric analysis was conducted by TGA Q500 (TA Instruments). At least 4 mg of AlO_x/PIM-1 samples were placed in platinum sample holders for the analysis. Thermogravimetric analysis was conducted in 90cc/min flowing air. The sample chamber is firstly heated to 110 °C and then maintained at 110 °C for 60 min. The heating at 110 °C allows complete evaporation of solvent residues. At the end of this process, the sample weight is used as the dry sample weight. Then the sample temperature increases to 900.00 °C at 10.00 °C/min, which decomposes organic compounds (PIM-1) into gases. The weight of the inorganic residue (aluminium oxide) is obtained. It is worth noting that the weight of aluminium oxide is not necessarily the weight of AlO_x in the AlO_x/PIM-1 sample due to the potential oxidation.

2.5. Wet impregnation of PEI

PEI (Mw = 800 Da) was loaded into PIM-1 or AlO_x/PIM-1 samples via wet impregnation following the previous study.[5] Briefly, methanol solution of PEI was filled into the glass vial containing PIM-1 or AlO_x/PIM-1 samples temporarily. The mass of PEI was calculated based on the target PEI loading with the assumption that all the PEI was captured by PIM-1, which is a reasonable assumption for PEI solutions with a concentration lower than 5 wt.%.[5]

2.6. Nitrogen physisorption

BET surface area and pore size distribution were obtained from 77-K N_2 physisorption via BELSORP-max (MicrotracBEL). Before measurement, the PIM-1 and AlO_x/PIM-1 samples were

refreshed with methanol to eliminate any confounding aging effects and then dried at 110 ºC under vacuum for 12 hr.[21] PEI-loaded samples were dried at 80 ºC under vacuum for 12 hr.

2.7. Thermodynamic equilibrium CO_2 adsorption isotherms

Thermodynamic equilibrium CO_2 adsorption isotherms were measured by Micromeritics ASAP 2020 (Micromeritics Instrument Corporation). Samples were degassed under vacuum (< 0.005 mmHg, 110 °C) for 12 h prior to the experiment. Samples used for equilibrium CO_2 adsorption isotherm measurement were ground into fine powders to minimize the kinetic limitation.

2.8. Pseudo-equilibrium CO_2 adsorption

Pseudo-equilibrium CO_2 adsorption isotherms of the PEI/PIM-1 and PEI/AlO_x/PIM-1 composites were collected using Dynamic Vapor Sorption equipment (Surface Measurement Systems Ltd.). Small fractions of samples were loaded onto the microbalance, which was located in an airtight sample chamber. Prior to the experiment, high vacuum (<10^{-3} mmHg) and heat (80 °C) are applied to the whole system to desorb CO_2 and solvent from the sample. During the measurement, pure CO_2 was continuously delivered into the sample chamber at a constant flow rate and evacuated by a vacuum pump. The valve between the sample chamber and the vacuum pump was controlled by the computer to maintain a desired sample chamber pressure. The sample weights at a series of CO_2 pressure were recorded at equilibrium (weight change < 0.005% within 1 min) or within 1 hour to establish the adsorption isotherm.

Cyclic temperature-and-pressure swing adsorption was conducted to evaluate the cyclic stability of PEI/AlO_x/PIM-1 as a practical CO_2 capture material. The temperature-and-pressure swing adsorption is conducted via Dynamic Vapor Sorption equipment (Surface Measurement Systems Ltd.). The adsorbent is initially vacuum dried (<3×10^{-6} mmHg, 80 °C) for 6 hr to remove solvent residue. The dried sample is then exposed to 76 mmHg CO_2 (flue gas simulant) for 2 hours

following 6-hr vacuum regeneration (<3×10^{-6} mmHg) at 80 °C. Such adsorption-desorption cycles were conducted at least seven times.

2.9. Mercury porosimetry

The macropores and mesopores of the PIM-1 fibers were characterized via mercury porosimetry. The polymer structures were dried under vacuum at 80 °C for 12 hours to get rid of solvent residues. The dry samples are then characterized in an AutoPore IV (Micromeritics) porosimeter.

2.10. Solid-state 1H spin diffusion

Solid-state ^{1}H spin diffusion NMR experiments were conducted on a Bruker AV3-300 spectrometer operating at a ^{1}H frequency of 300 MHz. Prior to NMR experiments, samples were degassed in a vacuum oven at 110 °C and at 20 mmHg overnight and then immediately packed and sealed in the rotor to minimize the amount of adsorbed atmospheric water and CO_2. The experiments were performed and analyzed following the work of Mellinger et al.[22]

3. Results and discussion

3.1. Chemical properties of AlOx/PIM-1

In this work, the VPI process produces hybrid AlO_x / PIM-1 fibers (Figure 1) that are thoroughly infiltrated with 29 wt% amorphous AlO_x (Figure S2a).[17] VPI infiltrates the bulk of PIM-1 with amorphous alumina constituents rather than simply coating the surface.[17] According to solid-state ^{27}Al NMR (Figure 2a) and consistent with our previous results,[17] the majority of aluminium atoms in the AlO_x/PIM-1 (5 hr, 2 cycles) are octahedral aluminium (Al^{VI}, 92.6 %). Pentahedral aluminium (Al^{IV}) and tetrahedral aluminium (Al^{V}) account for 5.0 % and 2.4 %, respectively.

In this work, XPS spectra of the aluminium outer valance band (Figure 2b) is used to investigate the chemical properties of the aluminium compound created by VPI, which could influence the CO_2 adsorption mechanism of adjacent amine molecules.[10] The difference between the various aluminium compounds ($Al(OH)_3$, Al_2O_3, and AlO(OH)) can be revealed by observing the two-peak features in the 0-15 eV binding energy range.[23] Aluminium oxide spectrum (α-Al_2O_3) exhibits two major peaks at 0-15 eV (Figure 2b), while the spectra of aluminium hydroxides (e.g., nordstrandite) and aluminium oxyhydroxides (e.g., boehmite) exhibit a major peak at 7-8 eV associated with a minor peak at 11-12 eV.[23] Similar twin-peak features were observed in AlO_x/PIM-1 spectra, which were absent in PIM-1 spectra (Figure S2b). As indicated by the XPS spectra of the aluminium outer valance band (Figure 2b), the aluminium compounds in AlO_x/PIM-1 resemble both $Al(OH)_3$ and AlO(OH), which suggests that the infiltrated aluminium species are likely oxyhydroxides in nature. The formation of aluminium oxyhydroxide is further supported by hydroxyl groups observed in FTIR spectra of the hybrid fibers (Figure S2c, d).

The formation of amorphous aluminium oxyhydroxide instead of aluminium oxide can be attributed to the limited exposure cycles and the inorganic's confinement in the polymer's micropores (Figure S2e, f).[17] The sub-nanometer micropores of PIM-1 effectively inhibit the growth of metal oxide beyond a small inorganic cluster or potentially nanostrands intertwined amongst the pores.

3.2. Microporosity of PEI/AlO_x/PIM-1

The microstructure of the resultant composite fiber is imperative to the operation of these fibers in CO_2 adsorption. In this report, PIM-1 fibers were produced via a phase inversion approach.[8, 18] Owing to the spinodal decomposition process, the PIM-1 fibers possess hierarchical porosity (Figure S2e-g). Figure 1 shows the SEM images of the cross-section of a hierarchically porous

PIM-1 fiber. Interconnected macropores are distributed throughout the fiber, which minimizes the kinetic limitation for CO_2 transportation through the fiber. The PIM-1 macropores minimize the CO_2 characteristic diffusion length in the adsorber down to sub-micrometer levels, which accelerates the adsorption process. No intact skin layer surrounding the fiber was observed. The porous outer surface allows rapid gas exchange with the external atmosphere, which further improves the adsorption kinetics. The intrinsic micropores and mesopores of PIM-1 provide residence spaces for PEI and diffusion pathways for CO_2.

The microporosity of PIM-1, AlO_x/PIM-1, and corresponding representative PEI composites are investigated via cryogenic nitrogen physisorption (Figure 3a). Pristine PIM-1 contains interconnected micropores and mesopores formed by the inefficient packing of the polymer backbone (Figure S1e, f),[24] which is prone to swelling by plasticizing guest molecules. For instance, swelling of PIM-1 is observed at nitrogen relative pressures higher than 0.05 in the cryogenic isotherms (Figure 3a).[17, 21] As a comparison, AlO_x/PIM-1 is a more rigid hybrid nanoporous network and significantly inhibits the swelling-contributed nitrogen adsorption in the higher-pressure regions of the isotherm (Figure 3a). It is worth noting that AlO_x does not consume a large amount of pore volume from PIM-1. Pure PIM-1 possesses 0.48 cm^3/g micropore and mesopore volume (Table 1), and AlO_x/PIM-1 possesses 0.418 cm^3/g micropore and mesopore volume, which is 0.59 cm^3 per gram of PIM-1. We hypothesize that PIM-1 skeleton is not a rigid structure during VPI treatment and the infiltrated species and reaction byproducts "swell" the PIM-1 skeleton,[21] which creates additional pore volume to compensate the volume occupied by AlO_x. As a result, the rigidification of PIM-1 does not necessarily sacrifice the host's porosity. Based on these pore volumes, the theoretical maximum PEI loadings for pure PIM-1 and AlO_x/PIM-1 are 34 wt% and 31 wt%, respectively.[5]

If the pore structure of PIM-1 is rigid and free of pore plugging, 27 wt % PEI/PIM-1 is expected to occupy 74% PIM-1 pore volume and preserve 26% pore volume of the original PIM-1 (Figure 3b, Table 1). However, experimentally 27 wt % PEI/PIM-1 only preserve 30% pore volume of PIM-1 (0.016 cm^3/g total pore volume). The lower-than-expected remaining pore volume, which is referred to as pore volume preservation in the following text, can be contributed by (1) micropore blockage by PEI, and (2) pore collapse due to PEI plasticization. As a comparison, PEI/AlO_x/PIM-1 with comparable theoretical pore volume occupation (76 % theoretical pore volume occupation at 25 wt % PEI loading) possesses 0.033 cm^3/g total pore volume, which corresponds to 33% pore volume preservation. The enhancement of pore volume preservation due to AlOx infiltration is observed in both micropore and mesopore regimes. As shown in Table 1, at comparable theoretical pore volume occupations, 27 wt % PEI/PIM-1 preserves 4% of micropores and 6% mesopores of the PIM-1 skeleton, while 25 wt % PEI/AlOx/PIM-1 retains 9% of micropores and 12% mesopores of the AlOx/PIM-1 skeleton. The improved micropore and mesopore preservation in PEI-loaded AlOx/PIM-1 suggests less pore plugging or collapse, which preserves more diffusion pathways for CO2 into the PEI domains far from gas streams.

The PEI/AlO_x/PIM-1 composite preserves un-plugged micropores even at excessive PEI loading. Excessive PEI loading is defined as PEI loading higher than the theoretical maximum PEI loading calculated based on the micropores and mesopores, which is 34 wt % for PEI/PIM-1 and 31 wt % for PEI/AlO_x/PIM-1. When excessive PEI is loaded (35 wt %), macropores of the AlO_x/PIM-1 will also accommodate PEI (Figure S2f and S2g). It is worth noting that the overloaded 35 wt % PEI/AlO_x/PIM-1 still retains 6% micropores (0.009 cm^3/g), which is even higher than the micropore preservation of 27% PEI/PIM-1.

Solid-state ^{1}H spin diffusion NMR experiments were performed to probe the size of PEI domains within the AlO_x/PIM-1, which is not influenced by potential pore blockage. The interpretation of PEI domain size can be found in SI section 3. The characteristic length for PEI in PEI/AlO_x/PIM-1 with PEI loading below 31 wt %, the theoretically maximum PEI loading in micropores, was found to be approximately 2.0±0.1 nm (Figure S3, Table S1). This characteristic length suggests the preferential residence of PEI in small mesopores of AlO_x/PIM-1 instead of macropores formed by phase inversion. N_2 physisorption data suggests that PEI occupies both microporous and mesoporous spaces essentially completely, although the entrances to the microporous volumes may simply be blocked by PEI molecules. Moreover, PEI has the ability to mix directly with the AlO_x/PIM-1 in addition to residing in porous spaces within the host material (Figure S2i). These two factors suggest that we cannot definitively pinpoint the location of the PEI.

As a comparison, the characteristic length for PEI in 10 wt % PEI/PIM-1 was found to be approximately 2.1±0.1 nm. Despite the similarities in characteristic length, we hypothesize that the AlO_x/PIM-1 samples possess more stable micropores than PIM-1. This speculation of micropore stabilization is supported by shortened T_2 (transverse relaxation time) values for PEI/AlO_x/PIM-1 as compared to T_2 values measured for pure PIM/PEI systems (Table S1). At PEI loading in AlO_x/PIM-1 higher than 31 wt % (e.g., 35 wt %, 40 wt %), the PEI characteristic length increases to approximately 2.6±0.1 nm as a result of the abundant plasticizing agents and macropore filling (Figure S2g). By contrast, poor dispersion of PEI in SBA-15 at high loadings has been reported: PEI aggregates in the mesopores (7−8 nm) of SBA-15, resulting in low amine efficiency and slow adsorption kinetics.[25]

3.3. CO_2 adsorption properties of PEI/AlO_x/PIM-1

While the microstructure and PEI loading of the PEI/AlO_x/PIM-1 fibers is indeed promising, the most pertinent characteristic for this application is CO_2 adsorption. Supported PEI is known to be kinetically limited during adsorption and therefore can not utilize thermodynamic capacity for CO_2 (Figure S4, Table S2).[5] All adsorbent materials considered here were fabricated into practical fiber adsorbent morphology (Figure 1) and pseudo-equilibrium capacities that could be realized during a practical adsorption operation are shown in Figure 4a. The dual-mode adsorption model is then used to predict the equilibrium CO_2 capacity of PEI/AlO_x/PIM-1 composites (Figure S5). Figure 4b shows the model-fitted equilibrium CO_2 adsorption of PEI/AlO_x/PIM-1 composites.

First, the sorption isotherms of PIM-1 and AlO_x/PIM-1 without PEI loading are compared. Both exhibit a dual-mode CO_2 sorption isotherm (Figure 4a), which is typical for gas sorption by glassy polymers. Dual-mode sorption assumes a combination of: Langmuir-type adsorption by the micropores and Henry's law sorption by the dense polymer region. CO_2 sorption in pure PIM-1 and AlO_x/PIM-1 results primarily from interaction between CO_2 and nitrile groups in the dense polymer regime. This interaction predominately results in Henry's law sorption with similar behaviors for both systems.[5, 26] However, the contribution of Langmuir-type adsorption to AlO_x/PIM-1 is higher than that in PIM-1 (Figure S5-S6, Table S3). The result indicates that the aluminium oxyhydroxide is more CO_2-philic than nitrile groups of PIM-1, which leads to enhanced Langmuir-type adsorption and overall higher CO_2 capacity.

Next, the influence of increasing PEI loading in PEI/AlO_x/PIM-1 composites was investigated under sub-excess PEI loading conditions. Under sub-excess PEI loading conditions (<35 %), the CO_2 capacity of PEI/AlO_x/PIM-1 increases with the PEI loading through the entire CO_2 pressure span. The change of the adsorption isotherm is most significant in the low-pressure range (<300

mmHg), which is particularly beneficial for practical CO_2 capture from flue gas (10-14% CO_2 concentration) and air (400 ppm CO_2 concentration). As the PEI loading increases (but remains sub-excess, < 35 %), the dual-mode CO_2 isotherm is gradually dominated by Langmuir-type adsorption. This indicates PEI is loaded into the micropores and effectively captures CO_2, resulting in increased Langmuir-type contribution to the overall CO_2 sorption.[5]

Further increasing PEI loading to excess PEI (41 wt %) decreases the CO_2 capacity of PEI/AlO_x/PIM-1, suggesting that excess PEI molecules accumulate at the external surface of the AlO_x/PIM-1 fibers and inhibit the exposure of internal amine groups to CO_2. However, excess PEI loaded (41 wt %) PEI/AlO_x/PIM-1 exhibits increased apparent CO_2 capacity at elevated temperatures (Figure S7), which suggests kinetic limitations due to excessive PEI loading.

The analysis of dual-mode adsorption model parameters provides additional insight into the microstructure of PEI/AlO_x/PIM-1 composites. In general, Henry's law sorption contribution, $\boldsymbol{k_{d,i}}$, decreases as PEI loading increases in both PEI/AlO_x/PIM-1 and PEI/PIM-1. This can be explained by the reduced accessibility of the dense PIM-1 regime. CO_2 is known to "crosslink" PEI and forms an impermeable coating on the microporous walls of AlO_x/PIM-1 or PIM-1 at higher partial pressures of CO_2.[5] The decreasing rate of $\boldsymbol{k_{d,i}}$ as PEI loading increase is less significant in PEI/AlO_x/PIM-1 ($\Delta \boldsymbol{k_{d,i}} / \Delta w_{PEI}$ = -1.26×10^{-4} mmol·g^{-1}·mmHg^{-1}·%$_{PEI}^{-1}$) than in PEI/PIM -1 ($\Delta \boldsymbol{k_{d,i}} / \Delta w_{PEI}$ = -2.32×10^{-4} mmol·g^{-1}·mmHg^{-1}·%$_{PEI}^{-1}$) as shown in Figure S5a and Figure S5b. This result suggests that aluminium oxyhydroxide nanostrands may inhibit the formation of defect-free PEI coating on the micropore walls and, therefore, make the dense polymer region more accessible to CO_2.

Next, the Langmuir adsorption contribution parameters $\boldsymbol{c_{H,i}}$ and $\boldsymbol{b_i}$, are investigated. For PEI/PIM-1 and PEI/AlO_x/PIM-1 $\boldsymbol{c_{H,i}}$ is associated with the total amount of amine groups that can be utilized for CO_2 capture. At the same PEI loading, the Langmuir adsorption contribution parameters, $\boldsymbol{c_{H,i}}$ and $\boldsymbol{b_i}$, of PEI/AlO_x/PIM-1 are higher than that of PEI/PIM-1, which suggests that aluminium oxyhydroxide nanostrands help expose amine groups or perhaps cooperatively interact with the amine groups.[10] The Langmuir adsorption contribution parameters, $\boldsymbol{c_{H,i}}$ and $\boldsymbol{b_i}$, of PEI/AlO_x/PIM-1 reach their maximum around the theoretical full-pore-filling PEI loading, 31 wt %, which indicates the efficient PEI loading limitation of AlO_x/PIM-1. The analysis of Langmuir adsorption contribution (porosity design) and Henry's law sorption (amine-molecule design) provides a hypothetical design strategy for the next-generation CO_2 adsorption materials: abundant rigid micropores and well-dispersed amine groups should be combined to maximize the CO_2 capacity of adsorbent materials.

3.4. Amine efficiency of PEI/AlO_x/PIM-1

Amine efficiency can be used to evaluate how efficiently the amine groups are used in CO_2 capture, which is defined as CO_2 adsorption capacity (mmol/g) normalized by the specific nitrogen atom quantity in the composite (mol/g). Pseudo-equilibrium amine efficiencies (Figure 5a) represent how effective the amine groups can be used during real adsorption applications. In contrast, model-fitted thermodynamic amine efficiencies (Figure 5b) represent how effective the amine groups can be used if infinite adsorption time can be provided.

The reported ratio of primary/secondary/tertiary nitrogens of the branched PEI used in this study is 44:33:23.[27] Since tertiary amines do not appreciably contribute to dry CO_2 adsorption and ammonium carbamate formation in dry conditions consumes two adjacent amine groups, the

highest amine efficiency possible is 380 mmol/mol.[5, 27] The infiltration of AlO_x significantly increases the amine efficiency. Figure 5a shows pseudo-equilibrium amine efficiencies of PEI/AlO_x/PIM-1 in comparison with PEI/PIM-1. At low PEI loadings (e.g., <15 wt %), amine efficiency for PEI/AlO_x/PIM-1 increases with an increase of PEI loading. We hypothesize that the PEI molecules are loosely dispersed in the micropores at low loadings. At 15 wt %, PEI/AlO_x/PIM-1 exhibits a nearly 100% amine efficiency increase over PE/PIM-1 in the low CO_2 pressure region (< 100 mmHg). Increasing the PEI loading may reduce the distance between two adjacent free amine groups, which facilities the formation of ammonium carbamate (one CO_2 and two adjacent amine groups) and increases the amine efficiency. At high PEI loadings (25-41 wt%), amine efficiency for PEI/AlO_x/PIM-1 decreases with the increase of PEI loading. At such high PEI loadings, the theoretical pore filling has exceeded 80%. Further, PEI loading results in pore plugging and denser amine group packing, which kinetically reduces amine efficiency (Figure S7-S8).

Additionally, PEI/AlO_x/PIM-1 samples with low PEI loading (e.g., 13 wt% and 15 wt%) reach the theoretical upper limit at 300 mmHg CO_2 pressure and apparently exceed it as pressure increases. At 300 mmHg, Henry's law sorption in dense PIM-1 is negligible (Table S2) and can be excluded as a possible rationale. Therefore, two hypotheses can explain this phenomenon. First, the infiltrated AlO_x nanostrands inhibit the densification of PEI molecules and expose more amine groups to CO_2 molecules. Second, the hydroxyl groups on AlO_x nanostrands may influence the carbamate formation and change the adsorption mechanism. Further investigation is required to explain the amine efficiency improvement.[10, 28, 29]

3.5. Performance comparison with state-of-the-art PEI-based adsorbents

PEI/AlO_x/PIM-1 at 15-35% PEI loading exhibits outstanding amine efficiency and competitive CO_2 capacity, while higher capacity adsorbents exist in the literature. Table 2 summarizes the CO_2 capacity of different state-of-the-art PEI-based materials in the flue gas regime (76 mmHg CO_2 partial pressure, 10% CO_2 flue gas simulant) measured at temperatures from 25 °C to 35 °C. When compared to state-of-the-art PEI-based adsorbents, 15-35 wt% PEI/AlO_x/PIM-1 exhibit higher CO_2 capacities relative at comparable PEI loadings (Figure 6). For instance, PEI/SBA-15 at 25 wt% PEI loading has been reported to exhibit 0.85 mmol/g CO_2 capacity at 25 °C.[1] As a comparison, PEI/AlO_x/PIM-1 at 25% PEI loading achieves 122% - 145% of this CO_2 capacity (1.04 mmol/g pseudo-equilibrium capacity and 1.23 mmol/g theoretical equilibrium capacity, Figure 4) at 35 °C, and is expected to achieve 1.26 mmol/g theoretical equilibrium capacity at 25 °C (Figure S7-S8,). At 25% PEI loading, PEI/AlO_x/PIM-1 achieves higher amine efficiency (35 °C pseudo-equilibrium: 183.33 mmol/mol; 35 °C equilibrium: 216.81 mmol/mol; 25 °C equilibrium: 221.83 mmol/mol) than PEI/SBA-15 (25 °C equilibrium: 149.60 mmol/mol) as shown in Table 2.

The outstanding amine efficiency of PEI/AlO_x/PIM-1 at 15-35% PEI loadings may be attributed to the improved microscopic dispersion of PEI within the AlO_x/PIM-1. As discussed in section 3.2, the sizes of PEI domains within the AlO_x/PIM-1 (PEI loading < 31%) is 2.0±0.1 nm (Figure S3, Table S1), which is smaller than the PEI domains in PIM-1 (2.1±0.1 nm) or SBA-15 (7−8 nm).[25]

Owing to the limitation of microporous volumes, the amine efficiency of PEI/AlO_x/PIM-1 decreases at PEI loadings higher than 31%. For instance, mesoporous alumina with 38.1 % PEI loading capture 1.73 mmol/g CO_2 at 25 °C and 76 mmHg CO_2 pressure. As a comparison, the 35 % PEI/AlO_x/PIM-1 achieves 1.19 mmol/g pseudo-equilibrium capacity and 1.46 mmol/g

equilibrium capacity (Figure 4, Table 2) at 35 °C and 76 mmHg CO_2 pressure. Under such overloading conditions, PEI/AlO_x/PIM-1 is not superior to classical PEI-loaded mesoporous materials: 35 °C equilibrium amine efficiency for 35% PEI/AlOx/PIM-1 is 183.54 mmol/mol, while 25 °C equilibrium amine efficiency for 38.1% PEI/mesoporous alumina is 199.77 mmol/mol. The lower CO_2 capacities and amine efficiency can be attributed to pore plugging; i.e., over-loaded PEI plugs the micropores of AlO_x/PIM-1, but mesoporous alumina has larger mesopores to accommodate more PEI with a lower possibility of pore plugging. Despite the high CO_2 capacity of 49% PEI/mesoporous alumina, its low amine efficiency (174.11 mmol/mol) potentially resulted by PEI agglomeration suggests that mesopores are not perfect residence for amine molecules.

In terms of equilibrium CO_2 capacity, PEI/AlO_x/PIM-1 is not the best among PEI-based adsorbents. However, it exhibits the highest amine efficiency among all state-of-the-art PEI-based adsorbents. When PEI is not overloaded and plugs the pores of AlO_x/PIM-1 (15-31 wt% PEI loading), PEI/AlO_x/PIM-1 exhibits higher amine efficiencies than other CO_2 adsorbents at the same PEI loadings. The exceptional amine efficiency indicates that AlO_x/PIM-1 is the most effective PEI support. The comparison between PEI/AlO_x/PIM-1 and PEI-loaded hard oxides provides a hypothetical design guide for next-generation amine-based adsorbent materials: (1) polymeric micropores or organics-decorated micropores should be utilized to achieve better mass transfer of CO_2 and potentially improved dispersion of amine molecules as well as better exposure of amine groups, (2) higher micropore volume is required to accommodate high amine molecule loadings, (3) rigid micropores should be utilized to resist the plasticization of amine molecules.

3.5. Stability of PEI/AlO_x/PIM-1

PEI/AlO_x/PIM-1 is also shown to be a stable material for the standard CO_2 capture operation. 12 temperature-and-pressure swing adsorption cycles were also conducted to evaluate the cyclic stability of PEI/AlO_x/PIM-1 as a practical CO_2 capture material (Figure S9). Figure 7 shows the kinetic uptake curves for 35% PEI/AlO_x/PIM-1. Over 12 cycles of sorption-regeneration, the adsorbent lost approximately 4% of CO_2 uptake capacity, which is comparable to the loss observed in cyclic tests for PEI-loaded hard oxides[1, 11, 30] and polymers[5, 31]. Such typical capacity loss is often attributed to irreversible urea formation instead of PEI evaporation, which is only 0.4% weight loss after 12 cycles (Figure S9b).

4. Conclusions

This work developed a new amine-based solid sorbent material, PEI/AlO_x/PIM-1, which consists of PEI, aluminium oxyhydroxide, and PIM-1. Hierarchically porous PIM-1 fiber is infused with amorphous aluminium oxyhydroxide via vapor phase infiltration and then loaded with PEI via wet impregnation. Owing to the solution-processibility of PIM-1, novel mass transfer contactor geometries (e.g., hollow fiber contactor, monolith-type contactors, etc.) beyond traditional pellet-based contactors can be applied to achieve heat integration, pressure drop minimization, and mass transfer optimization, which improves the energy efficiency of CO_2 adsorption systems. Compared with pure PIM-1, AlO_x/PIM-1 possess micropores with improved resistance to plasticizing amine molecules (PEI), which enables high PEI loading (up to 41%) and good dispersion. CO_2 adsorption isotherms, amine efficiency, and cyclic adsorption stability have been explored. PEI/AlO_x/PIM-1 composite exhibits outstanding amine efficiency and comparable CO_2 capacity when compared with classical PEI-loaded inorganic supports. This work suggests that materials with abundant

semi-rigid organics-based micropores could be better supports than mesoporous materials for dispersing functional materials at nanoscale. This material design principle could be deployed for micro-/mesoporous polymers, novel dispersive functional materials, and other challenging applications.

SCHEMES

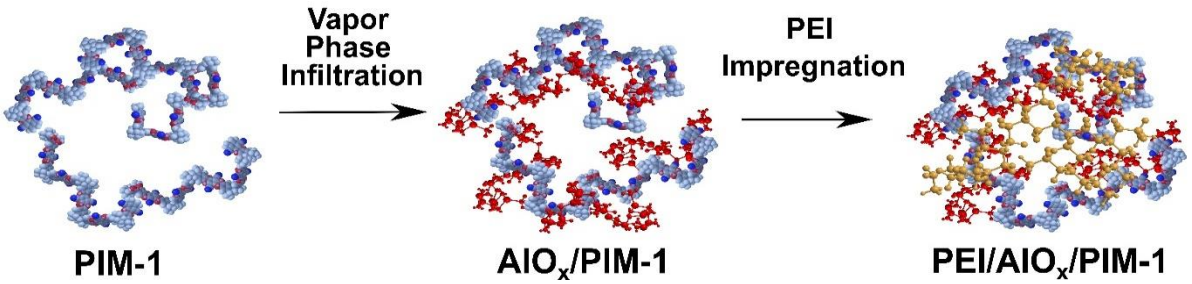

Scheme 1. The facile fabrication of PEI/AlO_x/PIM-1 structure.

FIGURES

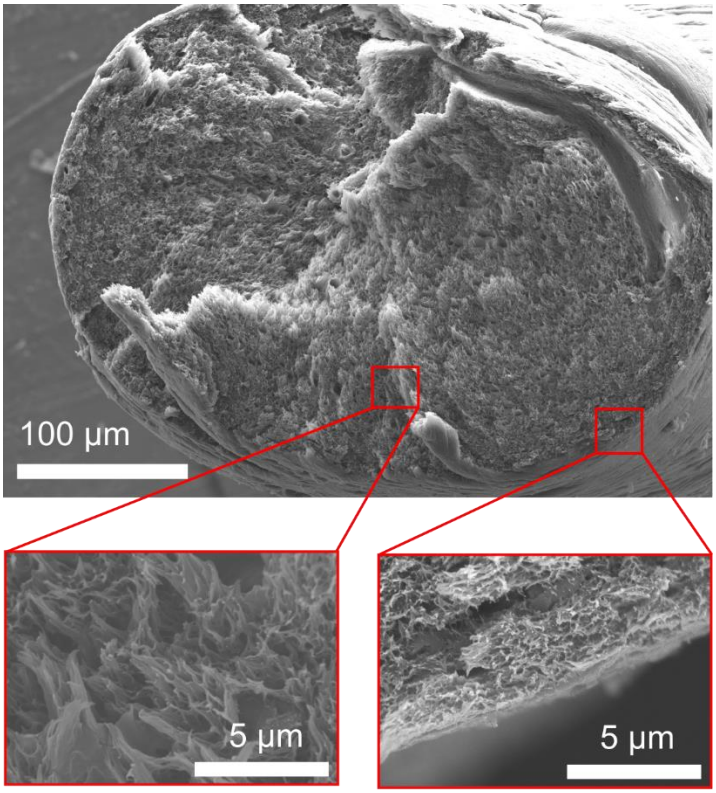

Figure 1. SEM images of the hierarchically porous AlOx/PIM-1 fibers used in this study.

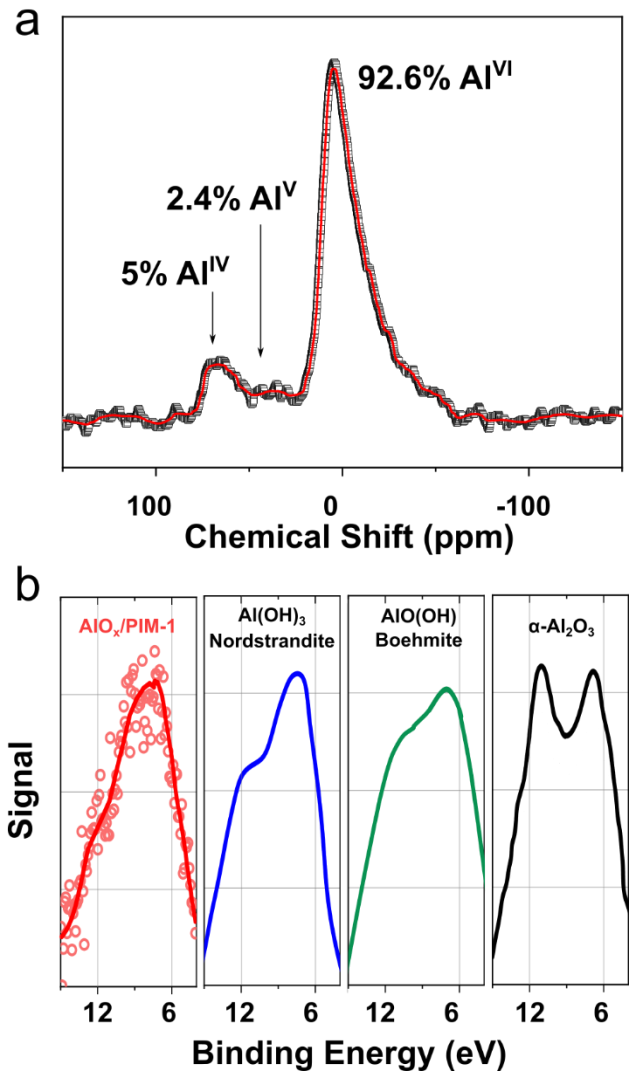

Figure 2. (a) Solid-state ^{27}Al NMR spectra and (b) valence band XPS of AlO_x/PIM-1 with linear-baseline correction compared with valence band spectra of Nordstrandite, Boehmite, and alpha alumina.[23]

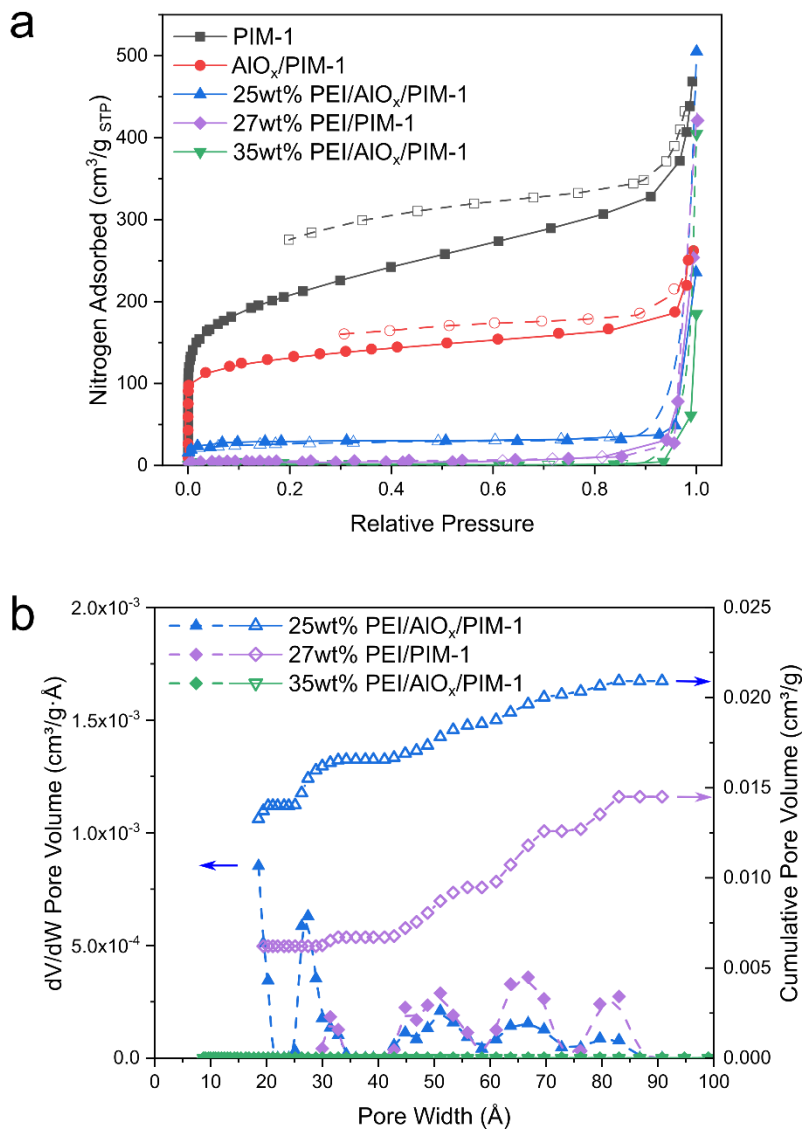

Figure 3. (a) Nitrogen physisorption at 77 K of PEI/AlO_x/PIM-1 and PEI/PIM-1 at different PEI loading (solid symbols: adsorption; open symbols: desorption). (b) Pore size distribution calculated via NLDFT model using the nitrogen physisorption isotherms (solid symbols: dV/dW pore volume; open symbols: cumulative pore volumes). Lines were used to guide eye.

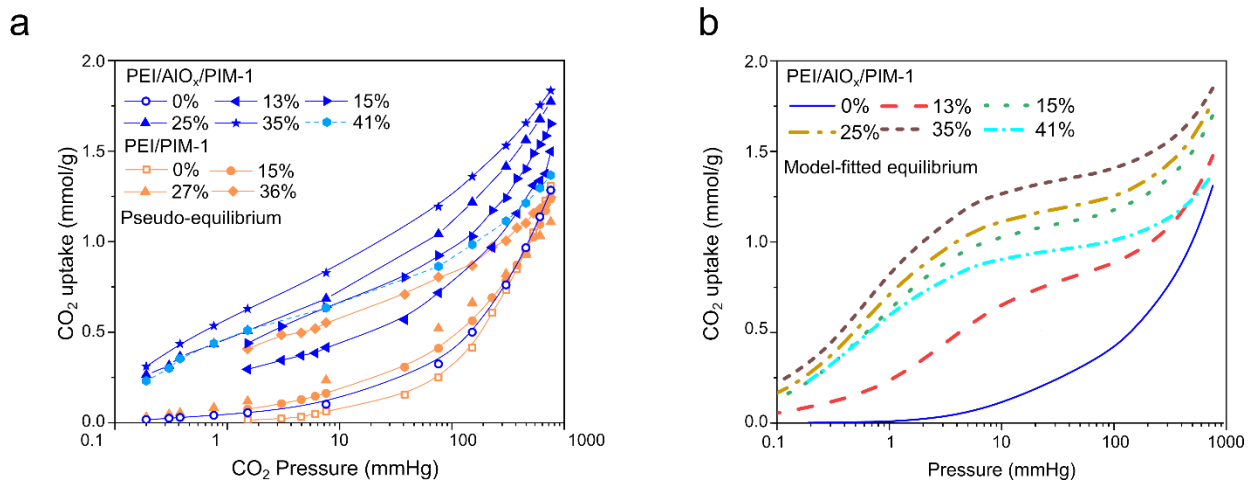

Figure 4. (a) Pseudo-equilibrium CO_2 adsorption isotherms at 35 °C for PEI/AlO_x/PIM-1 fibers and PEI/PIM-1 fibers as a function of PEI loading in weight percent of total mass. (b) equilibrium CO_2 adsorption isotherms predicted by dual-mode model at 35 °C for PEI/AlO_x/PIM-1 fibers and PEI/PIM-1 fibers as a function of PEI loading in weight percent of total mass. The solid and dashed lines were used to guide eye.

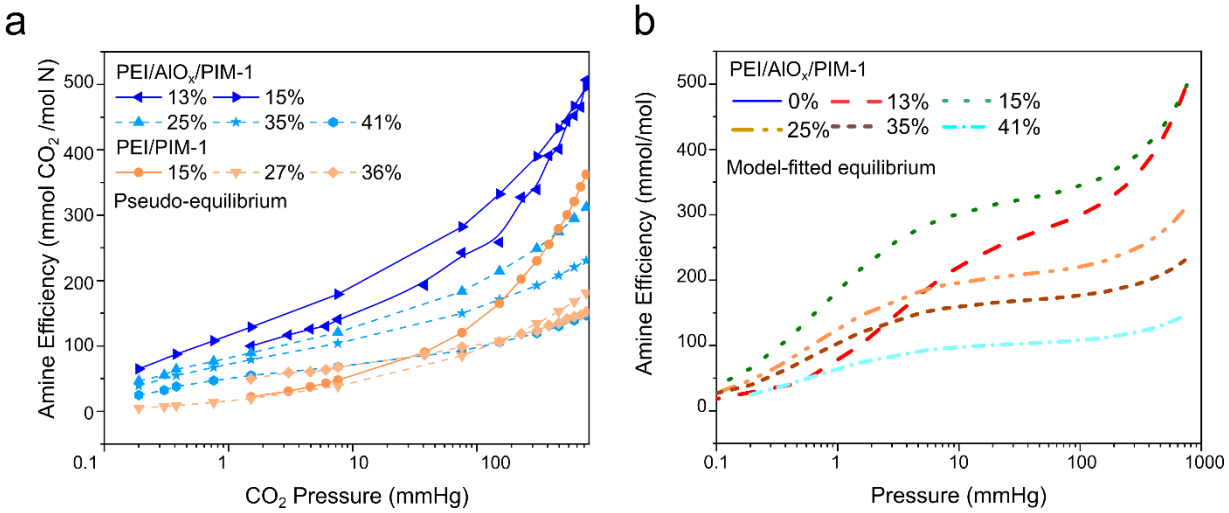

Figure 5. (a) Pseudo-equilibrium amine efficiencies at 35 °C for PEI/AlO_x/PIM-1 fibers and PEI/PIM-1 fibers as a function of PEI loading in weight percent of total mass. (b) Model-fitted

equilibrium amine efficiencies at 35 °C for PEI/AlO_x/PIM-1 fibers as a function of PEI loading in weight percent of total mass. The solid and dashed lines in (a), (b), (e), (f) were used to guide eye.

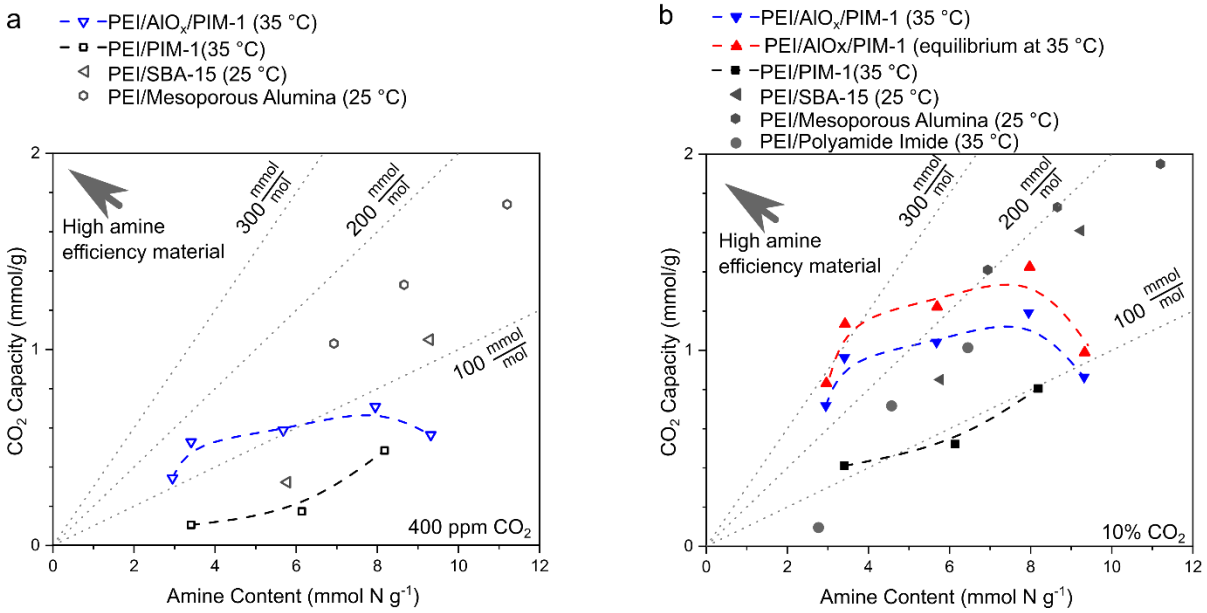

Figure 6. Comparison of CO_2 capacity and amine efficiency (denoted by the dot lines) of PEI/AlO_x/PIM-1 with state-of-the-art PEI-loaded materials (PEI/SBA-15,[1] synthesized mesoporous alumina,[1] PEI-Functionalized polyamide imide[15]) under (a) 400 ppm CO_2 and (b) 10% CO_2. The dashed lines were used to guide the evolution of CO_2 capacity of PEI/AlO_x/PIM-1 and PIM-1 at different amine loadings. Equilibrium CO_2 capacities of PEI/AlO_x/PIM-1 are experimentally measured for 7.95 mmol/g amine content and predicted via dual-mode adsorption model for the rest of the amine contents. The arrows at the left-up corner indicate the commercial-attractive high amine-efficiency materials in the plots.

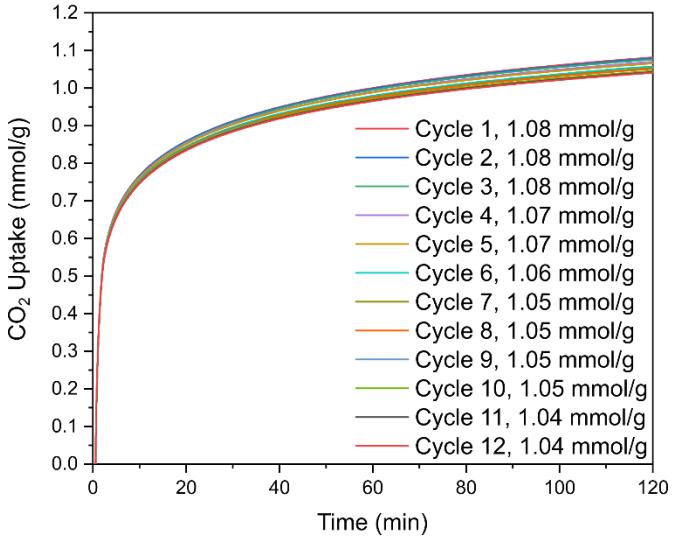

Figure 7. Cyclic Dynamic CO_2 uptake curves from 76 mmHg CO_2 on 35 wt % PEI/AlO_x/PIM-1 over 2 h of adsorption at 35 °C followed by 2 h of desorption at 110 °C in pure N_2 over the course of 12 temperature-and-pressure swing cycles.

TABLE of CONTENTS.

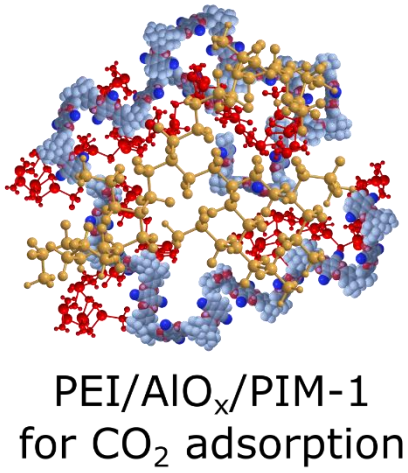

TABLES.

Table 1. Pore structure analysis of representative PEI/PIM-1 and PEI/AlO_x/PIM-1 composites

	PIM-1	27% PEI/PIM-1	AlO_x/PIM-1	25% PEI/AlO_x/PIM-1	35% PEI/AlO_x/PIM-1
Micropore Volume (cm^3/g)	0.232	0.006	0.208	0.014	0.009
Mesopore volume (cm^3/g)	0.248	0.010	0.210	0.019	0.000
Total Meso-Micro Pore Volume (cm^3/g)	0.480	0.016	0.418	0.033	0.009
Total pore volume preservation	-	30%	-	33%	37%
Micropore Volume Reduced (cm^3/g)	-	0.163	-	0.194	0.199
Micropore Volume Preservation	-	4%	-	9%	6%
Mesopore Volume Reduced (cm^3/g)	-	0.171	-	0.173	0.192
Mesopore Volume Preservation	-	6%	-	12%	0
Total Meso-Micro Pore Volume Reduced (cm^3/g)	-	0.334	-	0.281	0.263
Volume Occupied by PEI (cm^3/g)	-	0.257	-	0.238	0.333
Pore Volume Reduction due to Blockage or Collapse (cm^3/g)	-	0.077	-	0.042	NA[b]

[a] Determined via NLDFT model
[b] Overloaded PEI reside in external surfaces of the composite, which makes the calculation not applicable

Table 2. Performance comparison with state-of-the-art PEI-based adsorbents (76 mmHg CO_2 partial pressure, 10% CO_2 flue gas simulant)

Adsorbent	PEI Loading	Pseudo-equilibrium CO_2 capacity (mmol/g)	Equilibrium CO_2 capacity (mmol/g)	Pseudo-equilibrium amine efficiency (mmol/mol)	Equilibrium amine efficiency (mmol/mol)	Temperature (°C)
PEI/AlO_x/PIM-1	13%	0.72	0.86 [a]	243.04	290.66	35
	15%	0.96	1.15 [a]	282.16	337.28	
	25%	1.04	1.23 [a]	183.33	216.81	
	35%	1.19	1.46	149.96	183.54	
	41%	0.86	0.99 [a]	92.60	106.35	

PEI/PIM-1	15%	0.41	0.62	120.34	181.87	35
	27%	0.52	0.71	84.95	115.70	
	36 %	0.80	0.95	98.33	116.11	
PEI/PIM-1[5]	21%		1.15		240.95	35
	25%		0.97		170.72	
PEI-600-PAI[15]	20%		0.73		161.15	35
	12%		0.07		24.91	
	29%		1.00		152.21	
PEI/SBA-15[1]	25%		0.85		149.60	25
	40%		1.61		177.10	
PEI/Mesoporous Alumina[1]	31%		1.41		203.46	25
	38%		1.73		199.77	
	49%		1.95		174.11	

[a] Estimated via dual-mode model (SI section 2)

Supporting Information.

The Supporting Information is available free of charge.

Supplementary characterization including thermogravimetric analysis, XPS, FTIR, porosimetry, CO_2 sorption isotherm analysis, CO_2 sorption kinetic analysis, heat of CO_2 adsorption analysis, amine efficiency analysis, determination of the characteristic length of PEI domains, detailed temperature-and-pressure swing CO_2 adsorption. (PDF)

AUTHOR INFORMATION

Corresponding Author

Ryan P. Lively *

* E-mail: ryan.lively@chbe.gatech.edu.

Author Contributions

The manuscript was written through contributions of all authors. All authors have given approval to the final version of the manuscript.

Funding Sources

This material is based upon work supported by the National Science Foundation (DMREF-1921873). This work was performed in part at the Georgia Tech Institute for Electronics and Nanotechnology, a member of the National Nanotechnology Coordinated Infrastructure, which is supported by the National Science Foundation (Grant ECCS-1542174). The NMR experiments were performed by JL at Georgia Tech NMR Center. EKM was supported by the Department of Defense (DoD) through the National Defense Science & Engineering Graduate Fellowship (NDSEG) Program.

ACKNOWLEDGMENT

This material is based upon work supported by the National Science Foundation (DMREF-1921873). This work was performed in part at the Georgia Tech Institute for Electronics and Nanotechnology, a member of the National Nanotechnology Coordinated Infrastructure, which is supported by the National Science Foundation (Grant ECCS-1542174). The NMR experiments were performed by JL at Georgia Tech NMR Center. EKM was supported by the Department of Defense (DoD) through the National Defense Science & Engineering Graduate Fellowship (NDSEG) Program.

ABBREVIATIONS

XPS, X-ray photoelectron spectroscopy; FTIR, Fourier-transform infrared spectroscopy; NMR, nuclear magnetic resonance; BET, Brunauer–Emmett–Teller; VPI, vapor phase infiltration.

REFERENCES

1. Chaikittisilp, W.; Kim, H.-J.; Jones, C. W., Mesoporous alumina-supported amines as potential steam-stable adsorbents for capturing CO2 from simulated flue gas and ambient air. *Energy & Fuels* **2011,** *25* (11), 5528-5537.
2. Yu, C.-H.; Huang, C.-H.; Tan, C.-S., A review of CO2 capture by absorption and adsorption. *Aerosol and Air Quality Research* **2012,** *12* (5), 745-769.
3. Figueroa, J. D.; Fout, T.; Plasynski, S.; McIlvried, H.; Srivastava, R. D., Advances in CO2 capture technology—the US Department of Energy's Carbon Sequestration Program. *International journal of greenhouse gas control* **2008,** *2* (1), 9-20.
4. Rochelle, G. T., Amine scrubbing for CO2 capture. *Science* **2009,** *325* (5948), 1652-1654.
5. Pang, S. H.; Jue, M. L.; Leisen, J.; Jones, C. W.; Lively, R. P., PIM-1 as a solution-processable "molecular basket" for CO2 capture from dilute sources. *ACS Macro Letters* **2015,** *4* (12), 1415-1419.
6. Rinker, E. B.; Ashour, S. S.; Sandall, O. C., Absorption of carbon dioxide into aqueous blends of diethanolamine and methyldiethanolamine. *Industrial & engineering chemistry research* **2000,** *39* (11), 4346-4356.
7. Ma, Y.; Zhang, F.; Lively, R. P., Manufacturing Nanoporous Materials for Energy-Efficient Separations: Application and Challenges. In *Sustainable Nanoscale Engineering*, Elsevier: 2020; pp 33-81.
8. Zhang, F.; Ma, Y.; Liao, J.; Breedveld, V.; Lively, R. P., Solution‐Based 3D Printing of Polymers of Intrinsic Microporosity. *Macromolecular rapid communications* **2018,** *39* (13), 1800274.
9. DeWitt, S. J.; Sinha, A.; Kalyanaraman, J.; Zhang, F.; Realff, M. J.; Lively, R. P., Critical comparison of structured contactors for adsorption-based gas separations. *Annual review of chemical and biomolecular engineering* **2018,** *9*, 129-152.
10. Hahn, M. W.; Jelic, J.; Berger, E.; Reuter, K.; Jentys, A.; Lercher, J. A., Role of amine functionality for CO2 chemisorption on silica. *The Journal of Physical Chemistry B* **2016,** *120* (8), 1988-1995.
11. Heydari-Gorji, A.; Belmabkhout, Y.; Sayari, A., Polyethylenimine-impregnated mesoporous silica: effect of amine loading and surface alkyl chains on CO2 adsorption. *Langmuir* **2011,** *27* (20), 12411-12416.
12. Siegelman, R. L.; Milner, P. J.; Forse, A. C.; Lee, J.-H.; Colwell, K. A.; Neaton, J. B.; Reimer, J. A.; Weston, S. C.; Long, J. R., Water Enables Efficient CO2 Capture from Natural Gas Flue Emissions in an Oxidation-Resistant Diamine-Appended Metal–Organic Framework. *Journal of the American Chemical Society* **2019,** *141* (33), 13171-13186.
13. Lively, R. P.; Chance, R. R.; Kelley, B.; Deckman, H. W.; Drese, J. H.; Jones, C. W.; Koros, W. J., Hollow fiber adsorbents for CO2 removal from flue gas. *Industrial & Engineering Chemistry Research* **2009,** *48* (15), 7314-7324.
14. Slater, A. G.; Cooper, A. I., Function-led design of new porous materials. *Science* **2015,** *348* (6238), aaa8075.

15. Li, F. S.; Qiu, W.; Lively, R. P.; Lee, J. S.; Rownaghi, A. A.; Koros, W. J., Polyethyleneimine‐functionalized polyamide imide (Torlon) hollow‐fiber sorbents for post‐combustion CO2 capture. *ChemSusChem* **2013,** *6* (7), 1216-1223.
16. Rouquerol, J.; Avnir, D.; Fairbridge, C.; Everett, D.; Haynes, J.; Pernicone, N.; Ramsay, J.; Sing, K.; Unger, K., Recommendations for the characterization of porous solids (Technical Report). *Pure and applied chemistry* **1994,** *66* (8), 1739.
17. McGuinness, E. K.; Zhang, F.; Ma, Y.; Lively, R. P.; Losego, M. D., Vapor phase infiltration of metal oxides into nanoporous polymers for organic solvent separation membranes. *Chemistry of Materials* **2019,** *31* (15), 5509-5518.
18. Zhang, F.; Ma, Y.; Kondo, Y.; Breedveld, V.; Lively, R. P., A guide to solution‐based additive manufacturing of polymeric structures: Ink design, porosity manipulation, and printing strategy. *Journal of Advanced Manufacturing and Processing* **2020,** *2* (1), e10026.
19. Jue, M. L.; Breedveld, V.; Lively, R. P., Defect-free PIM-1 hollow fiber membranes. *Journal of Membrane Science* **2017,** *530*, 33-41.
20. McGuinness, E. K.; Leng, C. Z.; Losego, M. D., Increased Chemical Stability of Vapor-Phase Infiltrated AlO x–Poly (methyl methacrylate) Hybrid Materials. *ACS Applied Polymer Materials* **2020,** *2* (3), 1335-1344.
21. Jue, M. L.; McKay, C. S.; McCool, B. A.; Finn, M.; Lively, R. P., Effect of Nonsolvent Treatments on the Microstructure of PIM-1. *Macromolecules* **2015,** *48* (16), 5780-5790.
22. Mellinger, F.; Wilhelm, M.; Spiess, H. W., Calibration of 1H NMR spin diffusion coefficients for mobile polymers through transverse relaxation measurements. *Macromolecules* **1999,** *32* (14), 4686-4691.
23. Thomas, S.; Sherwood, P. M., Valence band spectra of aluminum oxides, hydroxides, and oxyhydroxides interpreted by X. alpha. calculations. *Analytical Chemistry* **1992,** *64* (21), 2488-2495.
24. Thompson, K. A.; Mathias, R.; Kim, D.; Kim, J.; Rangnekar, N.; Johnson, J.; Hoy, S. J.; Bechis, I.; Tarzia, A.; Jelfs, K. E., N-Aryl–linked spirocyclic polymers for membrane separations of complex hydrocarbon mixtures. *Science* **2020,** *369* (6501), 310-315.
25. Holewinski, A.; Sakwa-Novak, M. A.; Jones, C. W., Linking CO2 sorption performance to polymer morphology in aminopolymer/silica composites through neutron scattering. *Journal of the American Chemical Society* **2015,** *137* (36), 11749-11759.
26. Budd, P. M.; Msayib, K. J.; Tattershall, C. E.; Ghanem, B. S.; Reynolds, K. J.; McKeown, N. B.; Fritsch, D., Gas separation membranes from polymers of intrinsic microporosity. *Journal of Membrane Science* **2005,** *251* (1-2), 263-269.
27. Hicks, J. C.; Drese, J. H.; Fauth, D. J.; Gray, M. L.; Qi, G.; Jones, C. W., Designing adsorbents for CO2 capture from flue gas-hyperbranched aminosilicas capable of capturing CO2 reversibly. *Journal of the American Chemical Society* **2008,** *130* (10), 2902-2903.
28. Didas, S. A.; Sakwa-Novak, M. A.; Foo, G. S.; Sievers, C.; Jones, C. W., Effect of amine surface coverage on the co-adsorption of CO2 and water: spectral deconvolution of adsorbed species. *The journal of physical chemistry letters* **2014,** *5* (23), 4194-4200.
29. Yue, M. B.; Sun, L. B.; Cao, Y.; Wang, Z. J.; Wang, Y.; Yu, Q.; Zhu, J. H., Promoting the CO2 adsorption in the amine-containing SBA-15 by hydroxyl group. *Microporous and Mesoporous Materials* **2008,** *114* (1-3), 74-81.
30. Sanz, R.; Calleja, G.; Arencibia, A.; Sanz-Pérez, E., CO2 adsorption on branched polyethyleneimine-impregnated mesoporous silica SBA-15. *Applied Surface Science* **2010,** *256* (17), 5323-5328.

31. Jung, H.; Jo, D. H.; Lee, C. H.; Chung, W.; Shin, D.; Kim, S. H., Carbon dioxide capture using poly (ethylenimine)-impregnated poly (methyl methacrylate)-supported sorbents. *Energy & fuels* **2014,** *28* (6), 3994-4001.